Chapter 7
Dynamic Mechanical Reliability Test and Analysis

Abstract Chapter 7 focuses on vibration and drop impact test investigation. Experimental testing and FEA of the vibration mode and frequency for clamped–clamped PCB assemblies were compared. Constant amplitude vibration fatigue tests were conducted for the FCOB assemblies and test data were developed for 3G, 5G, and 10G respectively. Variable amplitude vibration fatigue tests for an increasing block loading of 3G-to-5G-to-10G repeated loading was conducted to develop cumulative damage index (CDI) vibration fatigue analysis methods using board-level fatigue data and solder material-level fatigue data. The Global–Local Sub-modeling technique developed was used in a quasi-static vibration fatigue analysis method for predicting the vibration fatigue life of the block loading test results. Impact drop testing is increasingly employed by many electronic product manufacturers to evaluate the product reliability to accidental or repeated drop events. Impact drop test and solder joint reliability investigations for Pb-based and Pb-free soldered assemblies were investigated. Explicit dynamic FEA modeling and simulation of the board-level drop test were used to predict the transient vibration deformation and acceleration from the drop test result. Dynamic stress strain analysis of the solder joints reveals fairly high plastic strain range generated and fatigue life prediction confirms the low cycle fatigue failure mechanism.

Electronic products are subjected to vibration loading during transportation and handling operations. The vibration loads are generally very low and screening vibration tests on a sample of the product are routinely conducted. However, for high reliability electronic applications, where the electronic soldered assemblies are mounted on an automotive, military, or aircraft moving platform, vibration fatigue tests are required. Another challenging reliability problem for soldered electronic assemblies is in the portable electronics sector (i.e., hand phone), where design for reliability against accidental drops is a highly competitive selling point. Drop impact tests are often conducted to study the drop-induced failures in soldered board-level assemblies and product level. In this chapter, vibration, drop test, and analysis for board-level soldered assemblies are reported.

J.H.L. Pang, *Lead Free Solder: Mechanics and Reliability*,
DOI 10.1007/978-1-4614-0463-7_7, © Springer Science+Business Media, LLC 2012

7.1 Vibration Test and Analysis

Electronic equipment can be subjected to many different forms of vibration loading over a wide frequency range and acceleration levels [1]. The simplest form of periodic motion is harmonic motion, which is usually represented by a continuous sine wave on a plot of displacement versus time, and this type of vibration is often selected for testing electronic equipment. For vibration analysis, vibration mode and natural frequency of the vibrating body must be determined. The first harmonic mode often has the greatest displacement amplitude and usually the greatest displacement-induced stresses. Vibration-induced stress can usually lead to fatigue failure for electronic assemblies. Vibration fatigue failure of solder joints is often assessed for reliability using high cycle fatigue model, which is represented by an *S*–*N* curve. A specimen *G*–*N* curve, acceleration versus fatigue life, was determined based on vibration test results. Modal analysis using FEA for surface-mounted components on a printed circuit board (PCB) was conducted [2]. Model analyses using different models were performed. Two-level global-local modeling approach [3–5] gave accurate results compared to test results. The analyses by Basaran [6, 7], Chandaroy [8] and Zhao et al. [9] show that solder joints respond elastically mainly at room temperature vibration loading.

A flip chip on board (FCOB) assembly was selected for vibration test to analyze the dynamic response of the FCOB to sinusoidal vibration. The specimen and chip number are shown in Fig. 7.1. Six larger flip chip modules of 8.5 × 8.5 × 0.65 mm (*L* × *W* × *H*) silicon die with 388 I/Os and six smaller flip chip modules of 3.5 × 3.5 × 0.65 mm (*L* × *W* × *H*) silicon die with 48 I/Os were mounted on the PWB assembly, which is made of FR-4 of 185 × 150 × 1.13 mm (*L* × *W* × *H*) in size. The solder joints are eutectic 63Sn/37Pb solder with a diameter of 0.16 mm, ball pitch of 0.35 mm, and standoff height of 0.1 mm. A total of four test boards were tested to different acceleration levels to assess the reliability of FCOB assembly subjecting to constant G-level and block G-level loading. Board 1 for varying amplitude test, including 3G, 5G, and 10G (G is gravity acceleration) blocks, Board 2, 3, 4 for constant 3G, 5G, 10G level vibration tests, respectively.

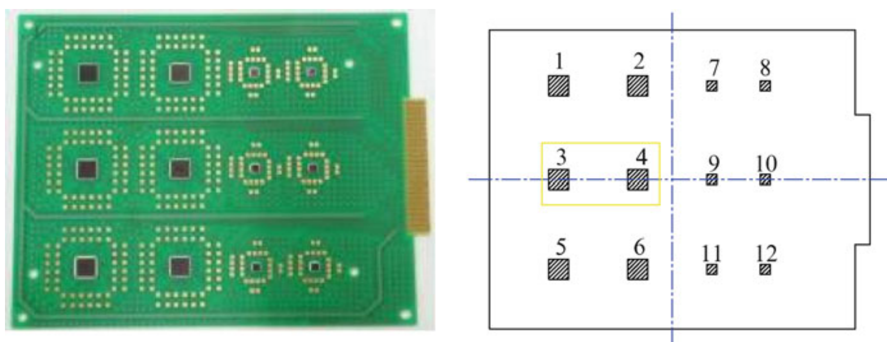

Fig. 7.1 FCOB assembly schematics and silicon chip number

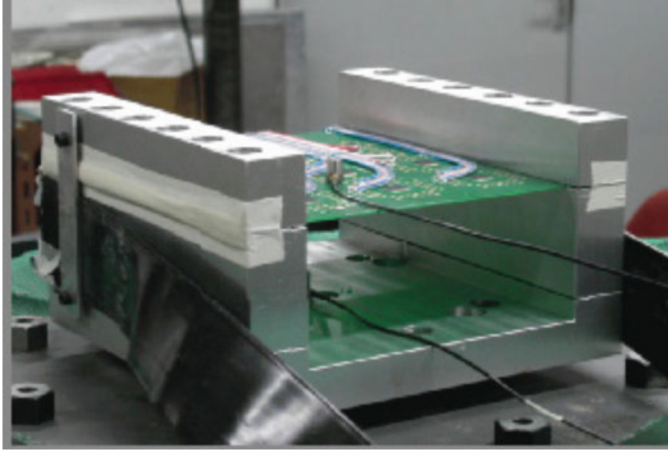

Fig. 7.2 Setup of the vibration test

Vibration tests of specimens were accomplished by using electrodynamic shaker and vibration control software. Two accelerometers were used in the test to determine the dynamic response of the specimen subjected to vibration, one for fixture and the other for PWB, thus the vibration transmissibility of the PWB can be determined when evaluated at different acceleration levels. In order to minimize the effect of the accelerometer's mass on the specimen, a miniature accelerometer (2 g of mass) was adopted. The specimen was clamped along two long opposite sides using aluminum fixture, which was bolted to the shaker header. This gives a clamped–clamped boundary condition for the specimen. The resistance change of the connecting loops to the solder joints was used to determine the failure of the solder joints. There are three loops for each larger flip chip, except for chip 6, with outer, middle, and inner loops. There is only one outer loop for each smaller chip and chip 6. A total of 22 loops were monitored simultaneously by the monitoring device called the Event Detector during vibration test. The threshold of the Event Detector was preset before the test. Any resistance change exceeding a preset threshold with minimum duration of 0.1 μs can be detected by the Event Detector. In general, 50% increase of resistance was used as a rule to determine the threshold setting. Figure 7.2 shows the setup of the vibration test.

The resonance frequency-scanning test was conducted first with sweep sine from 20 Hz to 1,000 Hz. The first order natural frequency of 194 Hz is determined by scanning test. The transmissibility of the specimen can be estimated using the following formula

$$T = \frac{G_{out}}{G_{in}}, \tag{7.1}$$

where G_{out} is the maximum acceleration measured at the center of the specimen, and G_{in} is the acceleration amplitude of the sinusoidal excitation.

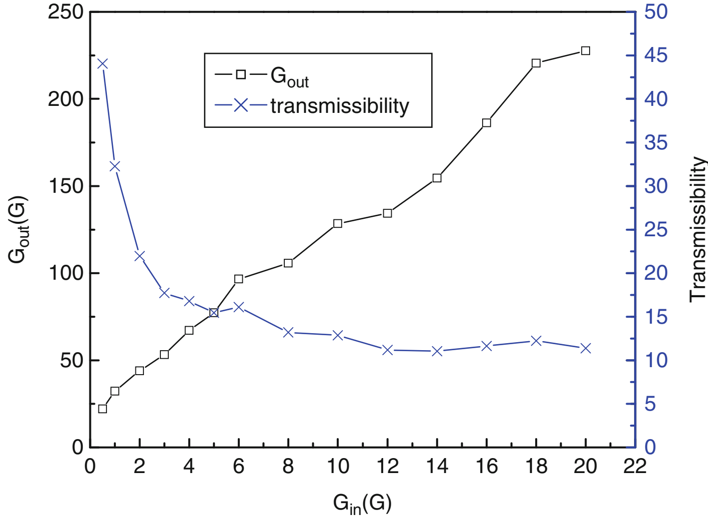

Fig. 7.3 Nonlinear relationship between G_{in} and G_{out}

According to Meirovitch [10], for a linear vibration system, its transmissibility should remain constant regardless of the any change in the input. However, the varying transmissibility, T, at different acceleration input was observed in test as shown in Fig. 7.3. The FCOB assembly under the out-of-plane sinusoidal excitation is not a linear vibration system. Yang et al. [11] showed that the PBGA assembly under out-of-plane vibration has similar nonlinear vibration effect.

The sweep frequency range was 10% around the fundamental resonance frequency, that is, from 175 to 215 Hz. For the varying block G-level vibration test, 3G, 5G, 10G level vibration tests were conducted in turn for each acceleration level of 5 h for same specimen. Constant G level vibration tests at 3G, 5G, and 10G were conducted for 200, 100, 36 h, respectively. Resistance change larger than 50% of initial resistance would be considered as a failure and recorded by the Event Detector, which continuously monitored the resistance of each daisy chain loop. The vibration cycles to failure were calculated based on the failure time recorded by the Event Detector and the average frequency of the sweep sinusoidal excitation. The test results for outer chains on the large chips are given in Fig. 7.4 and satisfy two-parameter Weibull distribution well. No failure results were obtained for the small chips components.

Table 7.1 shows the Weibull parameters together with the MTTF and first time to failure (FTTF) for three different G level tests. It can be seen from the table that the fatigue life reduces rapidly with increase of sinusoidal vibration acceleration amplitude.

From test results, a plot of G-level versus fatigue life can be obtained as shown in Fig. 7.5. In log-log scale, the liner relationship is clear. The fatigue model can be obtained based on G_{in}–N curve for FCOB assembly used in this study as expressed in the following equation

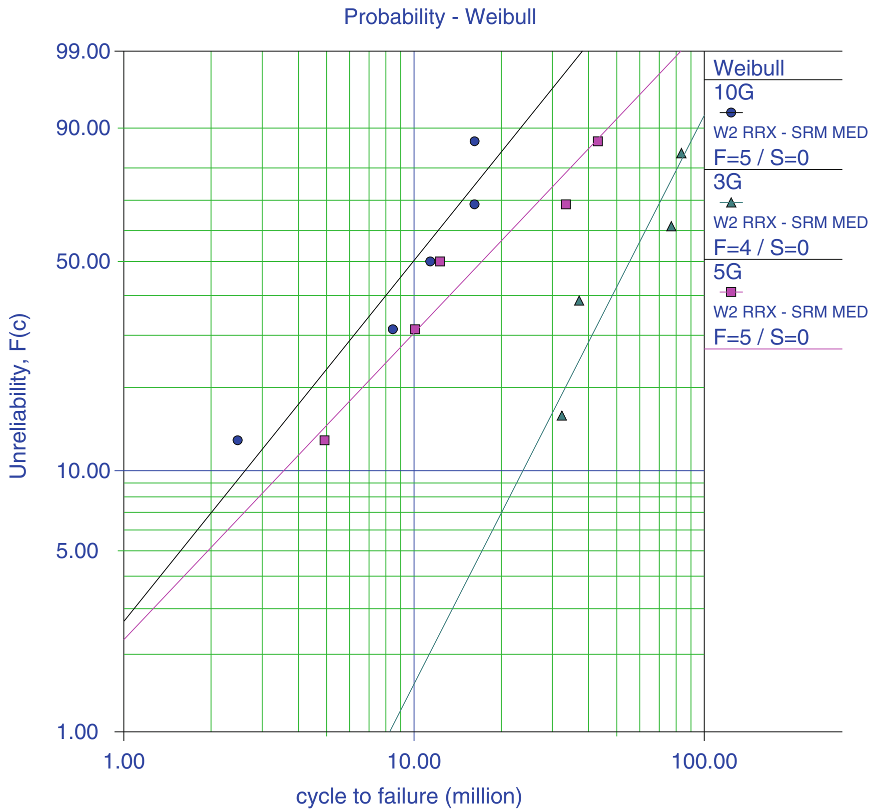

Fig. 7.4 Weibull plots of test results for different G_{in}

Table 7.1 Weibull parameters, MTTF and FTTF

G_{in}	$\eta(10^6)$	β	MTTF(10^6)	FTTF(10^6)
3G	65.30	2.22	57.84	32.30
5G	23.28	1.20	21.91	4.93
10G	12.89	1.41	11.73	2.47

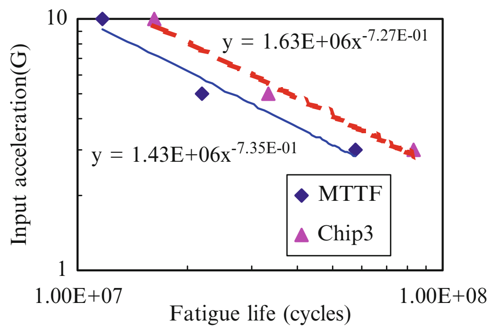

Fig. 7.5 Plot of input G-level versus fatigue life

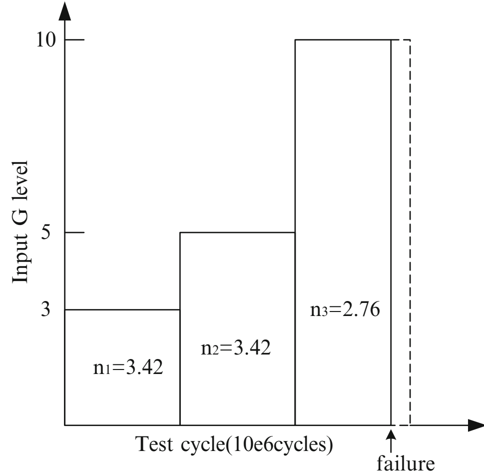

Fig. 7.6 Schematic of block G-level test for chip 3

$$
\begin{aligned}
A &= 1.43\mathrm{e}^{6} N^{-0.735} \text{ for } MTTF \\
A &= 1.63\mathrm{e}^{6} N^{-0.727} \text{ for chip 3,}
\end{aligned}
\tag{7.2}
$$

where A is input, G, N is fatigue life. Therefore, (7.2) can be used to predict fatigue life of FCOB assemblies subjected to different G-level input vibration tests.

For the electronic assembly subjected to different blocks of acceleration level (G-level) vibration test, the fatigue damage due to each acceleration level can be superimposed using the linear superposition method by Miner's law [12]. Miner's cumulative fatigue damage ratio is based on an analysis method that sums up the ratio of the actual number of fatigue cycles (n) accumulated in a specific element, in different environments, divided by the number of fatigue cycles (N) required to produce a fatigue failure in the same specific element in the same environment. When the ratios are added together, a sum of 1.0 or greater means that the fatigue life has been used up and should fail. The cumulative damage index (CDI) using Miner's cumulative damage law, assuming a linear summation given by

$$
\mathrm{CDI} = D_{\mathrm{total}} = \sum_{i=1}^{n} \frac{n_i}{N_i} \tag{7.3}
$$

Failure is assumed to occur at a more conservative value, such as $D_{\mathrm{total}} = 0.7$. For the varying G-level test, chip 3 and 4 were selected for the CDI analysis. The values of n_i are obtained from the varying G-level test result as shown in Fig. 7.6 for chip 3 and Fig. 7.7 for chip 4 while N_i values are equal to MTTF shown in Table 7.1. Substituting the data shown in Figs. 7.6 and 7.7 into (7.3), the CDI can be obtained:

$$
\begin{aligned}
\mathrm{CDI}_{\mathrm{chip3}} &= \frac{n_1}{N_1} + \frac{n_2}{N_2} + \frac{n_3}{N_3} = \frac{3.42}{57.84} + \frac{3.42}{21.91} + \frac{2.76}{11.73} = 0.451 \\
\mathrm{CDI}_{\mathrm{chip\,4}} &= \frac{n_1}{N_1} + \frac{n_2}{N_2} + \frac{n_3}{N_3} = \frac{6.84}{57.84} + \frac{6.84}{21.91} + \frac{3.65}{11.73} = 0.742
\end{aligned}
$$

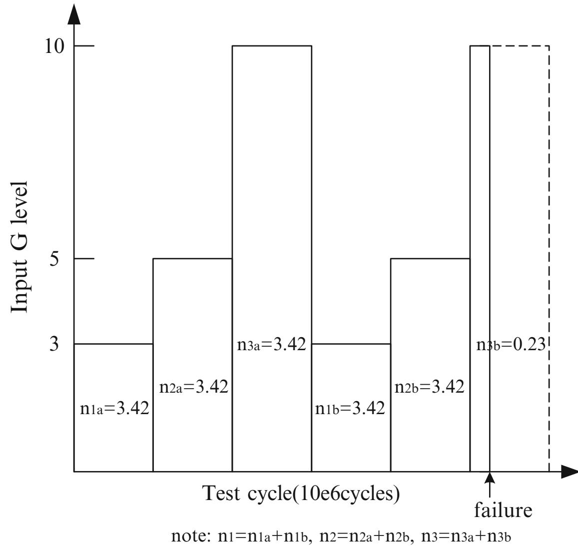

Fig. 7.7 Schematic of block G-level test for chip 4

From CDI values for chip 3 and 4, when the CDI was 0.451 and 0.742 for outer chain of chip 3 and 4, the failure occurred in these two chips, respectively. Using the CDI of unity is unconservative and a safety factor of 3 is recommended.

7.2 Finite Element Analysis for Vibration Test

Because the natural frequencies and mode shapes are very important parameters in the design of a structure for dynamic loading conditions, modal analysis to determine these parameters was conducted firstly. PWB was modeled as shell element in FE modal analysis. The clamped–clamped boundary condition was simulated according to the testing condition. First, the bare PWB without Flip Chip components attached was simulated for modal analysis to study the different variables effect such as material properties, element size. The FE model of the bear PWB is shown in Fig. 7.8. Table 7.2 shows the natural frequency results of first three modes for bare PWB when considering different variables. The element size has a very slight effect on the natural frequency of the bare PWB. In the subsequent analysis, the 5 × 5 mm shell element size was used. Actually, the FR-4 PWB has the orthotropic material properties. However, it can be seen from Table 7.2 that the effect of the orthotropic material properties on the natural frequencies is very slight so that the effect can be neglected.

In order to verify that a good approximation of PWB modal response can be made by considering the PWB as a bare unpopulated thin plate, four detailed modal analyses were conducted. In case 1, the Flip Chip components mounted on the PWB were modeled as distributed masses on the PWB. In case 2, the Flip Chip

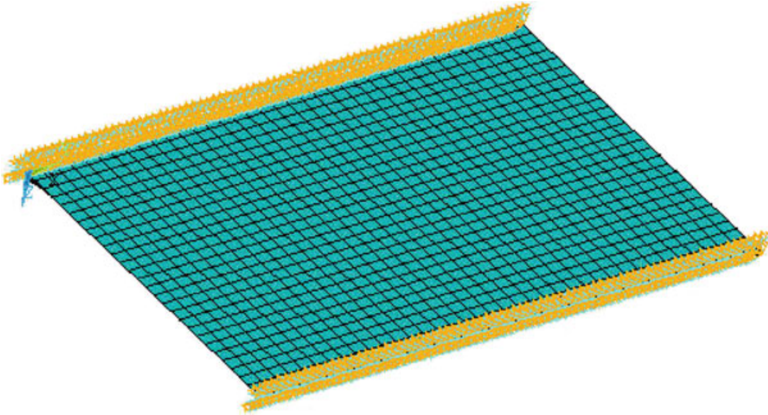

Fig. 7.8 Finite element model of bare PWB

Table 7.2 Natural frequency for bare PWB modal analysis

No.	*E* (GPa)	*v*	f1	f2	f3	Element size (mm × mm)
1	22	0.28	208	232	324	2.5 × 2.5
2	22	0.28	208	232	323	5 × 5
3	22	0.28	208	232	322	7.5 × 7.5
4	22	0.28	208	232	322	10 × 10
5	$E_x = 22$ $E_y = 22$ $E_z = 10$	$v_{xy} = 0.28$ $v_{yz} = 0.11$ $v_{zx} = 0.12$	208	232	322	5 × 5

components were modeled as concentrated masses at the center locations of the components on the PWB. In case 3, the Flip Chip components were modeled as solid part of the pure chip without considering the effects of the solder joint and underfill. In case 4, the IC chips were modeled as shell and the solder joints were modeled as effective two-node beam elements with equivalent stiffness of solder joint [5]. According to Steinberg [1], the fundamental resonance frequency for a PWB with the Clamped–Clamped boundary condition can be obtained from the following equation

$$f_n = \frac{3.55}{a^2}\sqrt{\frac{D}{\rho}}, \tag{7.4}$$

where

$$D = \frac{Eh^3}{12(1-\mu^2)}, \quad \rho = \frac{\text{Mass}}{\text{Area}},$$

$E = 22{,}000\ \text{N/mm}^2$, (Young's modulus),
$\mu = 0.28$, (Poisson's ratio),

Table 7.3 Comparison of the natural frequencies results

Mode	Bare PWB	Case 1	Case 2	Case 3	Case 4	Eq. (7.4)	Test
1	208	206	206	209	201	209	194
2	232	231	231	234	213		
3	323	321	321	326	272		

$h = 1.13$ mm, (thickness of the PWB),
$a = 140$ mm, (free side length of the PWB), and
$\rho = 2.147$ kg/m$^{2.}$

Table 7.3 shows the first three order frequencies of the PWB obtained from different methods. The frequencies obtained from case 1 and case 2 were slightly less than those from bare PWB because only the masses increased for the PWB while the stiffness did not change for PWB. It can be seen from Table 7.3 that the results of modal analysis have a good agreement among FEA, test and theory. Therefore, for PWB with Flip Chip assembly, a good approximation of PWB modal response can be made by considering the PWB as a bare unpopulated thin plate. The increase in stiffness of PWB due to the mounting of the components is offset by the increase in total mass the populated PWB. The same approximation can introduce more error for PWB with BGA assemblies because the contribution of the masses and stiffness of the BGA modules for PWB could not be ignored as the BGA modules have the larger volume and mass compared with Flip Chip modules. The first natural frequency obtained by case 4 has better agreement with the testing results.

A quasi-static analysis method was developed to calculate the stress strain behavior of the solder joints, which can be used for fatigue life prediction using high cycle fatigue model. The dynamic loading due to vibration was replaced by effective static loading in this method. According to Newton's second law, the pressure acting on the PWB or component can be obtained

$$p = \frac{F}{A} = \frac{mG_{\text{out}}}{A} = \frac{\rho v G_{\text{out}}}{A} = \rho t G_{\text{out}} g, \tag{7.5}$$

where m, ρ, v, A, t are mass, density, volume, area, thickness of PWB, or chip i, respectively. G_{out} is output acceleration in G (acceleration of gravity).

For constant G-level test, the pressure loading can be obtained from (7.4) and (7.5) when transmissibility is known. It is observed that transmissibility is not a constant value along transverse locations. The transmissibility was measured only for half of the PWB due to symmetry. Eight locations uniformly distributed shown in the Fig. 7.9 were selected to measure transmissibility of the PWB subjected to vibration. Figure 7.10 shows the transmissibility result for different locations at fundamental resonance frequency for 10G input test, and that a linear relationship between transmissibility and location is clear.

Sub-modeling technique was used in this quasi-static analysis because it is difficult to take board level simulation using full 3D model. Figure 7.11 shows the brief procedure for sub-modeling technique. For the whole model, only two

Fig. 7.9 Schematic of the location of the measured point

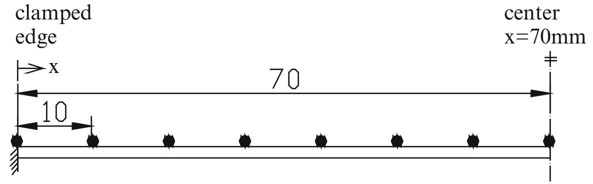

Fig. 7.10 Transmissibility at natural frequency for 10G test

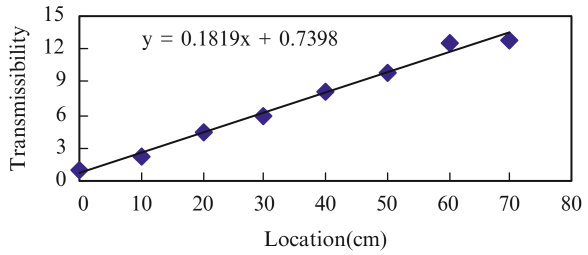

Fig. 7.11 Sub-modeling technique for vibration stress analysis

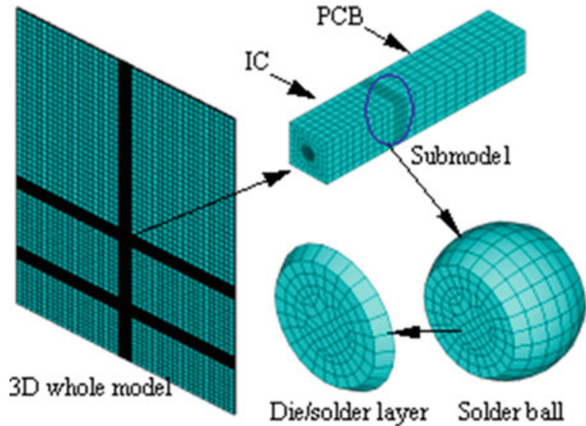

large chips numbered 3 and 4 shown in Fig. 7.1 distributed on center of PWB were selected and clamped–clamped boundary condition along two opposite longer sides was used. Elastic-plastic analysis for solder joint was used and no plastic strain occurs from result. The stress strain distribution for two chips was almost same, so only chip 3 was used for analysis. The outmost corner solder joint has the maximum stress, which means the first failure will occur in the outmost corner solder joint. Thus, sub-model was used to simulate the outmost solder joint. The stress-based high cycle fatigue approach was used to predict the fatigue life of component as shown below:

$$\sigma_{\mathrm{a}} = \sigma_{\mathrm{f}}'(2N_{\mathrm{f}})^{b}, \tag{7.6}$$

where σ_a = stress amplitude,

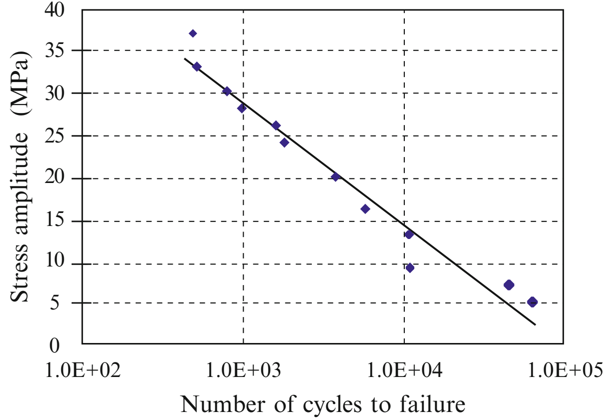

Fig. 7.12 High cycle fatigue S-logN curve for solder [13]

$\sigma_f{}'$ = fatigue strength coefficient,
b = fatigue strength exponent, and
$2N_f$ = reversals of failure (1 reversal = 1/2 cycle).

For eutectic Pb/Sn solder, the material constant $\sigma_f{}'$ and b can be determined by curve fitting shown in Fig. 7.12 using testing data by Yao et al. [13] and they are 177.1 MPa and −0.2427, respectively. For multi-axes stress situation, the equivalent von Mises stress is used to output the state of stress in the solder joint.

$$\sigma_{\mathrm{eff}} = \frac{1}{\sqrt{2}}\sqrt{(\sigma_1-\sigma_2)^2+(\sigma_2-\sigma_3)^2+(\sigma_3-\sigma_1)^2} \tag{7.7}$$

In order to minimize the effect of stress concentration, the volume-weight method was used to calculate the equivalent von Mises stress for the die/solder interface layer in which the failure commonly occurs first for FCOB assembly. Volume-weight average stress can be obtained by

$$\sigma_{ave} = \frac{\sum \sigma \cdot V}{\sum V} \tag{7.8}$$

Then fatigue life can be determined by (7.8) when stress amplitude was known. The frequency range from 175 to 215 Hz was used for vibration test. Different transmissibility occurs at different frequencies as shown in Fig. 7.13. Therefore, specimen was subjected to different effective pressures with different slop triangle distribution at utmost location during test. Miner's law shown in (7.3) was used and fatigue life can be predicted combining with (7.6). In this study, CDI of 0.5 was used. The fatigue life result comparisons between quasi-static method and testing for chip 3 are listed in Table 7.4. It can be seen that the quasi-static can give reasonable fatigue life prediction result compared to testing result, especially for lower G-level vibration test. By imitating *S–N* curve, the *G–N* curve can be

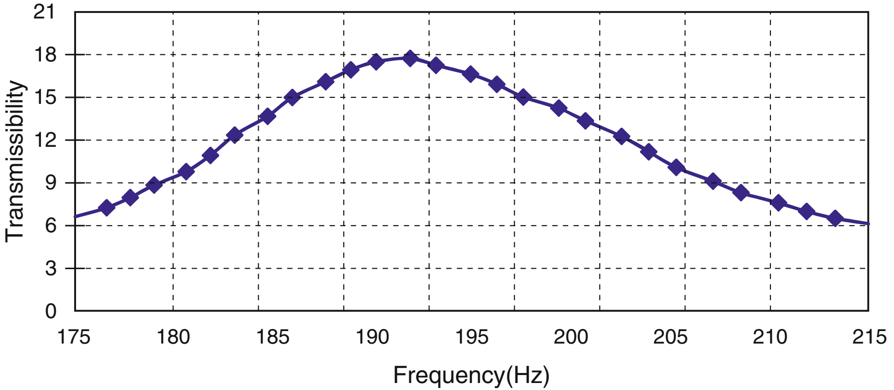

Fig. 7.13 Transmissibility versus frequency for 3G test

Table 7.4 Fatigue life comparisons for chip 3

G level	Test (1)	Prediction (2)	Factor (2/1)
3	8.34E + 07	1.10E + 08	1.32
5	3.34E + 07	2.57E + 07	0.77
10	1.62E + 07	2.61E + 06	0.16

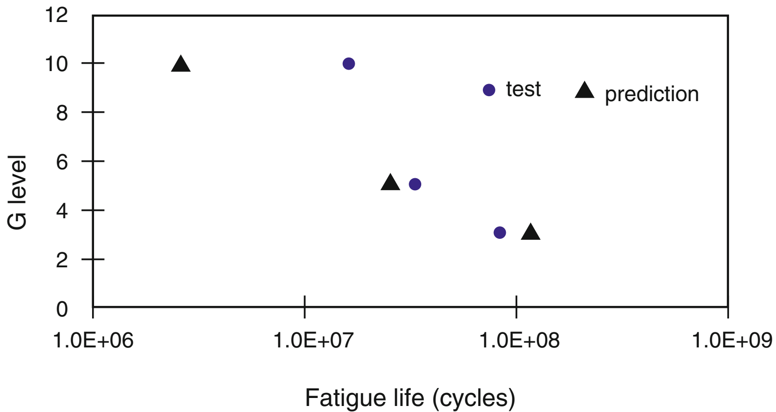

Fig. 7.14 G-N curve for different methods

obtained based on fatigue life result for different G-level test as shown in Fig. 7.14. Different CDI values were used to predict the flip chip solder joint fatigue life in order to investigate the CDI effect. The factor is defined as the ratio of fatigue cycles predicted by FEA to experimental fatigue cycles. Different factors corresponding to four CDI values of 1, 0.7, 0.5, and 0.33 were calculated and shown in Fig. 7.15. It can be seen that fatigue life prediction has a good agreement with test data for 5G vibration test.

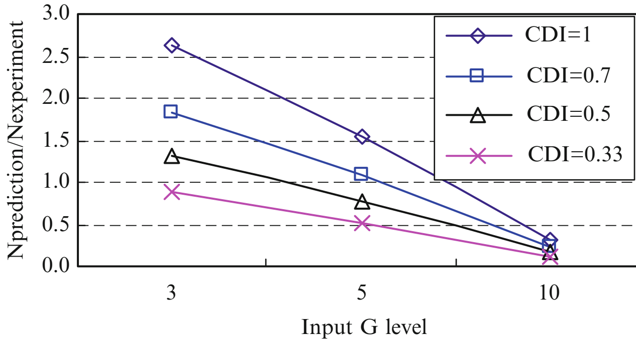

Fig. 7.15 CDI effect on fatigue life prediction

7.3 Drop Impact Test and FEA Modeling

Portable electronic devices like personal digital assistant (PDA) and mobile hand phone have to be designed to withstand drops. In these devices, flip chips are widely used to reduce weight and mounting size. Impact and drop studies of flip chip solder joints reliability are emerging research interests. The flip chip solder joints are subjected to operating conditions and accidental drop causing short-time stress from impact loading. Drop tests are often substituted in qualification testing of microelectronic devices by shock tests. In order to adequately mimic the drop test conditions, a short-term external acceleration is applied and should be well below the fundamental period of system's free vibrations. Otherwise, the response of the system can result in substantially higher curvatures and accelerations than that occurring during drop tests [14]. In the drop test, the measured maximum acceleration is often used as a criterion of the strength of structure in microelectronic products. The maximum acceleration of PCB board can reach to more than 1,000G when subjected to drop impact, but the displacement and strain of the PCB is relatively small. It is well known, however, that it is the maximum stress, not the maximum acceleration, which is responsible for the dynamic strength of a structure [15]. The dynamic reliability of portable electronic equipment relates to several external and product factors, which affect the forces and accelerations during impact [16] drop height, housing material, weight, shape, orientation at impact, and surface onto which it drops. Most drop heights used in the industry are 1 and 1.5 m. Yu et al. [17] show that the horizontal impact case of PCB is the most dangerous case for reliability of solder joints. The first order mode vibration is more dominant in dynamic fracture of solder joints than higher modes. There are mainly three types of drop tests in the electronic industry: (1) free fall product level; (2) free fall board level; and (3) controlled pulse drop at board level. Board level drop test is convenient to characterize the solder joint performance, as it is more controllable than product level drop test. Some researchers [18–20] have conducted board level drop tests to understand the response of solder joint to impact loading.

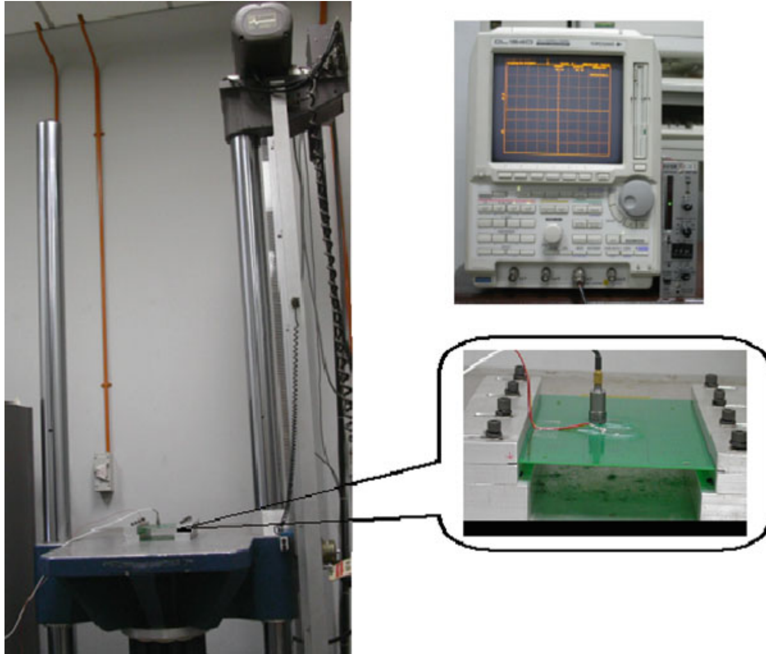

Fig. 7.16 Drop test setup and fixed specimen

Some researchers [21, 22] have conducted product level drop tests due to real drop events. In this study, free fall board level drop test was conducted.

In this study, FCOB assembly shown in Fig. 7.2 was selected for drop test to analyze the dynamic response of the FCOB to drop impact loading. The Lansmont Model 65/81-shock test machine is used to provide the free-fall drop test of board-level mounted with the flip chip packages. This machine can provide two types of shock pulse: half sine pulse and trapezoid pulse. The half sine pulse will be chosen for the excitation of the impact. The acceleration level of the half sine pulse is related to the drop height and mount of the felt pads. The duration of the pulse is adjustable, somewhat, by the addition or subtraction of the felt pads. The drop machine and specimen are shown in Fig. 7.16.

The drop table is an aluminum weldment with an assembled mass of approximately 190.5 kg. It has a 650 × 810 mm top-mounting surface, which is drilled and fitted with threaded inserts for test specimen mounting. The specimen of PCB with flip chip packages is attached to a metal table through aluminum fixture shown in Fig. 7.16. During impact, the longitudinal stress wave will travel in the table, when the wave travels into the PCB, it turns into the bending wave. The propagation velocity of the longitudinal stress wave in the table and fixture can be expressed as [23]

$$C_{\mathrm{L}} = \sqrt{\frac{E}{\rho}}, \tag{7.9}$$

Fig. 7.17 Marks on the specimen and fixture

where E is the Young's modulus and ρ is the density of the material. The velocity of the bending wave in the specimen may be expressed as

$$C_{\mathrm{b}} = \frac{\pi\gamma}{L}, \tag{7.10}$$

where $\gamma = \sqrt{D/\rho_a}$, D is the flexural modulus $Eh^3/12$, h is thickness of specimen, $\rho_a = \rho\, h$ is the area density of specimen, and L is the length of the free edge.

Usually, in the drop test, impact force, accelerations, drop velocity, and strains are measured. In this test, the strain gages and accelerometer affixed to the surface of the PCB desired location are used to measure the dynamic strain and acceleration of the specimen shown in Fig. 7.17. This specimen has the fundamental frequency of 195 Hz determined by the vibration test, which is equivalent to period of the 5.1 ms.

After every five drop tests, the continuity of the functional daisy chain net was checked using a multimeter. Failure criterion was electrical open of the daisy chain net. During the drop test, a high-speed camera was used to capture the images of the specimen movements. This camera has an ability to record up to 4,500 frames per second for immediate playback so that the image storage of extremely rapid events such as drop can be accurately carried out. Based on the results obtained by the high-speed camera, the position and shape of the specimen can be obtained. Furthermore, the velocities, accelerations, and flections of the specimen can be calculated by using the fundamental data of displacement. Before the drop test, some marks are attached on the specimen, which can make the data recorded easily by high-speed camera, shown in Fig. 7.17. Mark 4 is a reference point attached on the fixture, and Marks 1, 2, and 3 are located on the left side, center point, and right side of specimen edge, respectively.

In the first drop test, four felt pads were placed on the base surface to prevent metal-to-metal impact. The drop height is 1 m. The vertical relative displacements obtained from the high-speed camera are shown in Fig. 7.18. The data for a period of 20 ms were extracted for analysis. These relative displacements represent the displacement differences between the marks on specimen and mark on fixture. It can be seen from Fig. 7.18 that the motion of the specimen during the drop test is similar to the simple harmonic motion and maximum deflection along the specimen occurs at almost the same time, suggesting the existence of a dominant fundamental deformation mode. The vibration displacement range (2 × amplitude) of the center point marked by No. 2 shown in Fig. 7.18 is about 4.9 mm approximately. It can be

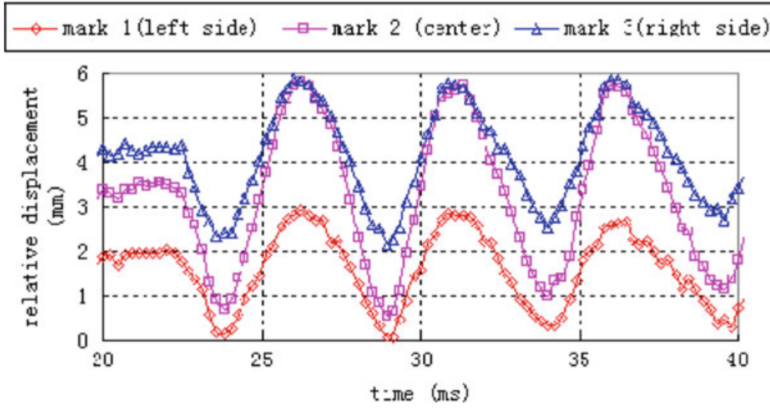

Fig. 7.18 Relative displacement of the specimen (camera)

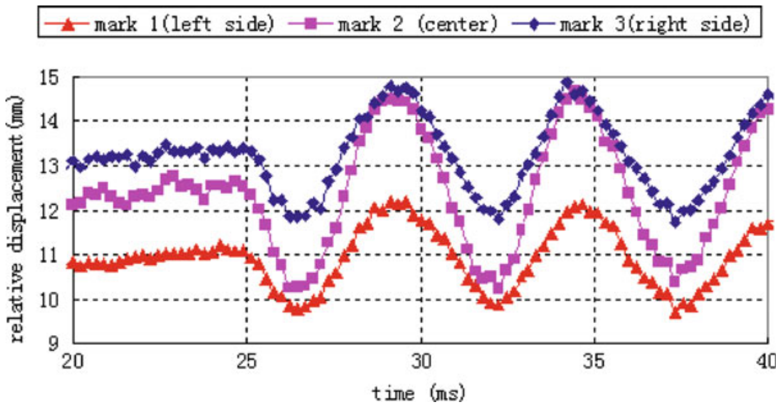

Fig. 7.19 Relative displacement of the specimen with wooden plate on drop base

seen from Fig. 7.18 that the vibration period of the specimen during and after impact is about 5.4 ms. This is equivalent to the frequency of 185 Hz and is close to the theoretical fundamental frequency of the PCB specimen of 195 Hz, for the first vibration mode shape under clamped–clamped condition tested.

A wooden plate was placed above the felt pads in order to vary the effect of the impact surface on the dynamic response of the specimen. The relative displacement of the specimen is shown in Fig. 7.19. The vibration displacement range of the center point of the specimen is equal to 4.4 mm and a vibration period of the specimen is about 5.7 ms. Compared with the results shown in Figs. 7.18 and 7.19, it is obvious that the wooden plate reduces the maximum vibration displacement and increases vibration period of the specimen, thus the maximum acceleration of the specimen will be reduced.

The acceleration of the specimen calculated from the data recorded by high-speed camera is shown in Fig. 7.20. It can be seen that the maximum acceleration occurs at

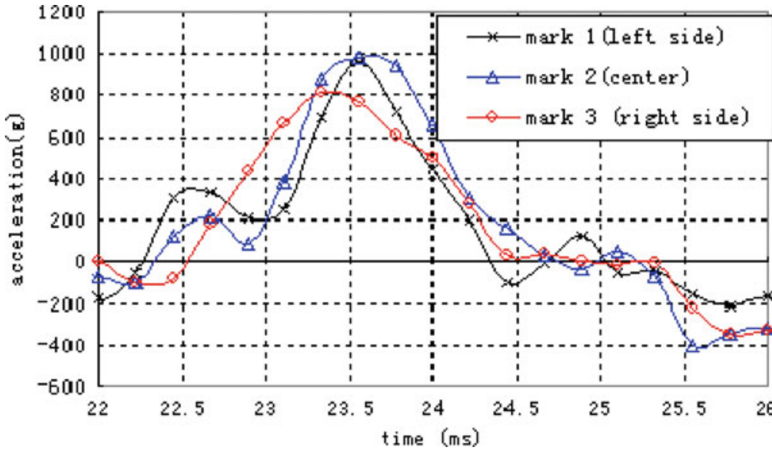

Fig. 7.20 Acceleration of the specimen (camera)

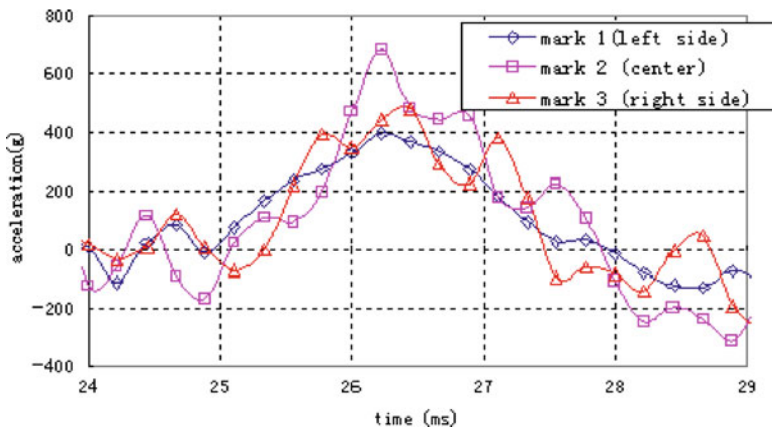

Fig. 7.21 Acceleration of the specimen (accelerometer)

the center of the specimen and the acceleration has a value of 981G. The relationship of the acceleration and time presents a half-sine shape and the duration of the impact is 2.5 ms. In addition, the acceleration can be measured directly by the accelerometer, and the results are shown in Fig. 7.21. Comparison with the results by camera shown in Fig. 7.20 and the accelerometer result in Fig. 7.21, the acceleration of the center point of the specimen has a magnitude of 980G and duration of 2.5 ms. The acceleration of the drop table is also measured during the impact period and is shown in Fig. 7.21. According to (7.9), the stress wave propagation velocity of the table reaches to 5,090 m/s, so the transition of the wave in the table is very fast and impact wave can travel through table to specimen in 0.06 ms. Therefore, the maximum accelerations of the specimen and drop table almost occur in the same

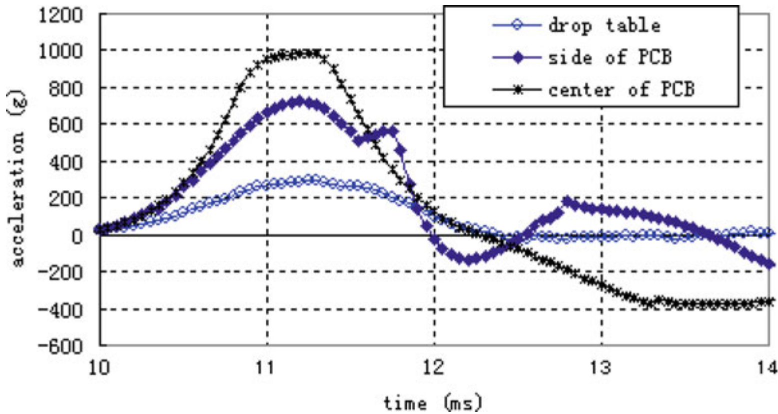

Fig. 7.22 Acceleration of the specimen with wooden plate on drop base

time, as can be validated from Fig. 7.21. It can be seen that the acceleration of the center point of the PCB specimen has a higher G magnitude compared to that of the side of the PCB and the drop table. Note that transient vibration of the PCB specimen continues even after the table approaches a stable state.

Figure 7.22 shows accelerations of specimen when a wooden plate was placed on the drop base. It can be seen that the maximum acceleration reduces to 700G for the center point and half-sine shape has a bigger duration of 3 ms compared with those results shown in Fig. 7.20 without wooden plate. Therefore, the soft drop base would reduce the maximum acceleration during impact and extend the duration of impact.

After more than 30 drops, no failure of solder joint was found based on the resistance measured. The FCOB assembly has good impact drop solder joint reliability performance due to underfill encapsulation. Other SMT assemblies, such as PBGA, CBGA, QFP, and TSOP board level assemblies may not be so resistant to drop impact tests.

The combination of numerical simulation and testing is the best approach to obtain failure analysis to understand the dynamic response of the electronic assembly on impact loading. It is a significant advantage for numerical simulation that it can pick up complete mechanical information at any location of analyzed object. Impact response is a typically transient phenomenon. In transient analysis with FEA, there are two basic algorithms for time integration methods: implicit and explicit methods. ANSYS has a LS-DYNA module for explicit-based problems and was selected for the simulation of the impact problem in this study. It has suitable element type, material model, and contact surface definition capabilities.

In the analysis, the specimen, fixture, table, and impact base are all simulated. The detailed model is shown in Fig. 7.23. Assume a rigid behavior for the drop base and bilinear kinematic hardening plasticity for the table, fixture, and specimen. The table and fixture are modeled using solid element, specimen using shell, and base using rigid shell. Some important information of the element, material properties is listed in the

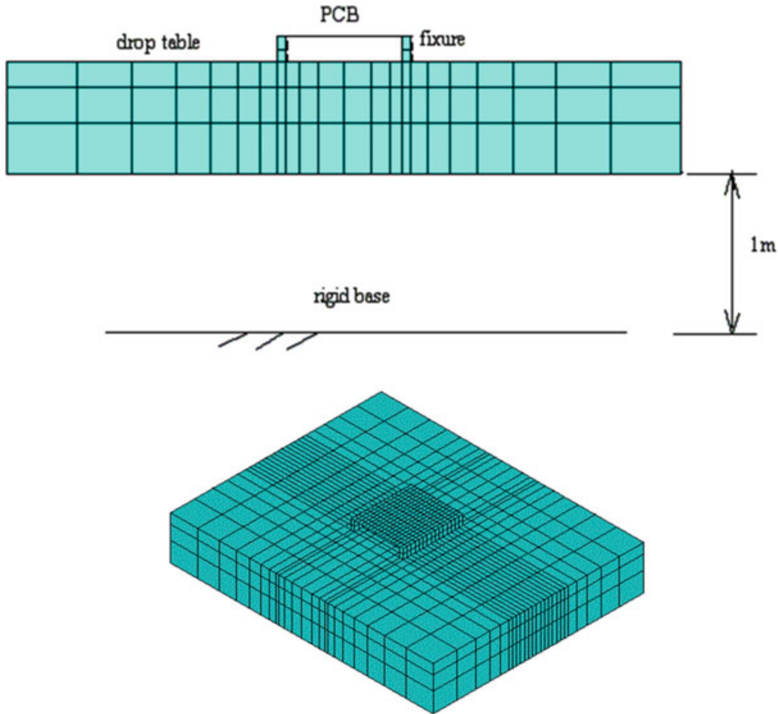

Fig. 7.23 Impact model and meshed fall part

Table 7.5 Element types and material properties of the model

Components	Table and fixture	Specimen	Drop base
Element type	Solid 164	Shell 163	Shell 163(rigid)
Density (kg/m^3)	2,700	1,900	7,800
Elastic modulus (GPa)	70	22	200
Poisson ratio	0.346	0.28	0.25

Table 7.5. A total of 1,921 elements and 2,836 nodes are included in this analysis. The simulation time is 50 ms, and 500 substeps are involved during this simulation period. During the free fall stage, the table and specimen is simply accelerating due to gravity. To save CPU time, apply an initial velocity of 4.43 m/s to simulate the free drop height of 1 m. 4.43 m/s is an approximation derived using $v = \sqrt{2gh}$, where v is the final velocity, g is the acceleration due to gravity, and h is the displacement of 1 m.

In order to interpret the dynamic response of the specimen on the drop test conveniently, some labels are marked in the Fig. 7.24 for specimen shell. Label C presents a central line, which also is a symmetric axis of the specimen shell. Label L1 and R1 present the outmost left line and right line, respectively, and they are symmetric about central line labeled mark C. The line labeled L2, located the middle position between line of L1 and line of C, is symmetric to the line labeled R2 about central line.

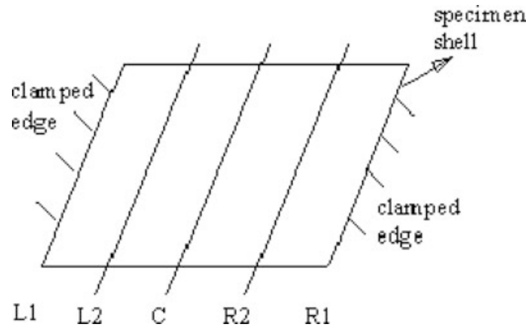

Fig. 7.24 Labels on the specimen

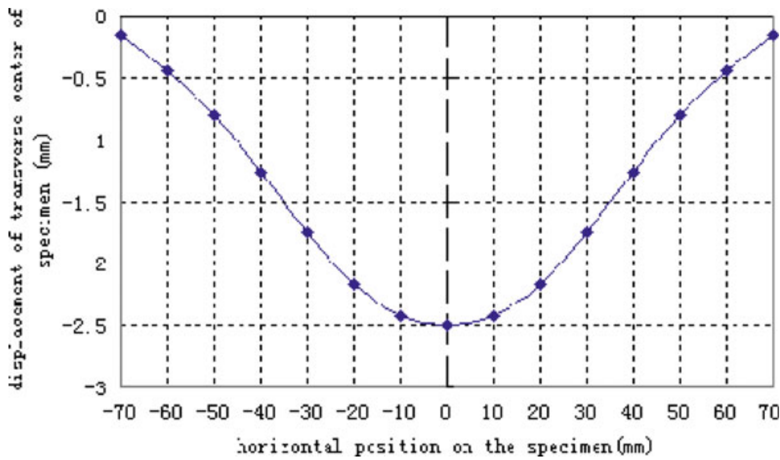

Fig. 7.25 Maximum relative displacement of the specimen

From the results, it was found that the specimen vibrates in the form of first order mode shape, so the displacements, velocities, and accelerations at the symmetric location of specimen have the similar trends and magnitude.

The deformation along the transverse direction of the specimen is shown in Fig. 7.25. It can be seen that the deformation is symmetric about the central line and this deformation shape is consistent with the first vibration mode. The maximum displacement of the center is about 2.5 mm, which agrees well with the result obtained by high-speed camera.

The symmetric deformation of the specimen during drop test can also be validated from the rotational angle shown in Fig. 7.26. It can be seen that the vibration shape of the specimen after impact exhibits the first vibration mode shape. For this type of drop test, we can consider that certain period vibration is induced by the impact force. Thus, drop test problem can be considered a transient vibration problem. It can be seen that the rotation angle decreases with the time increasing

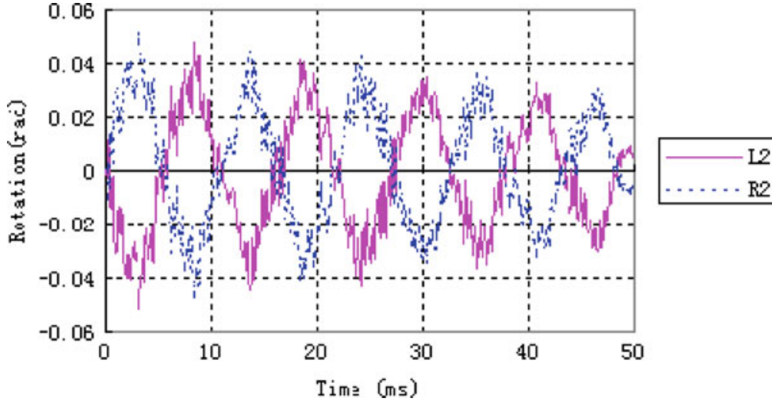

Fig. 7.26 Rotation angle of the specimen about horizontal axis

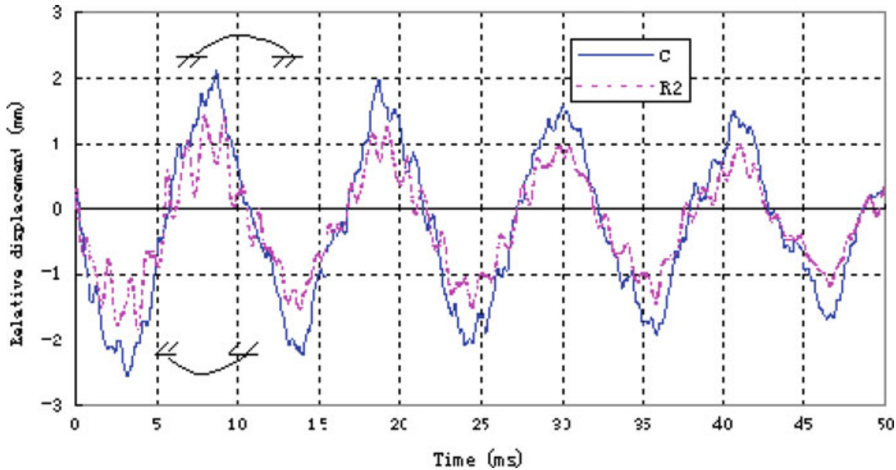

Fig. 7.27 Relative displacement–time relation of specimen

due to air damping. The vibration period of 10 ms can be obtained from Fig. 7.27, which is larger than that from high-speed camera.

The acceleration results of FEA are shown in the Fig. 7.28. The maximum acceleration of the specimen is 1,400G approximately, which is higher than the real maximum acceleration of 980G measured by the accelerometer during the drop test because of the effect of the rigid base used in the FEA. Taking the drop base as a rigid body without considering the effect of the felt pads induces the difference between the measured results and simulation. Further modeling study is needed to obtain more accurate simulation results for acceleration.

The simulation of the drop base as rigid body leads to overestimation of the acceleration at the center of the board compared to the measured response.

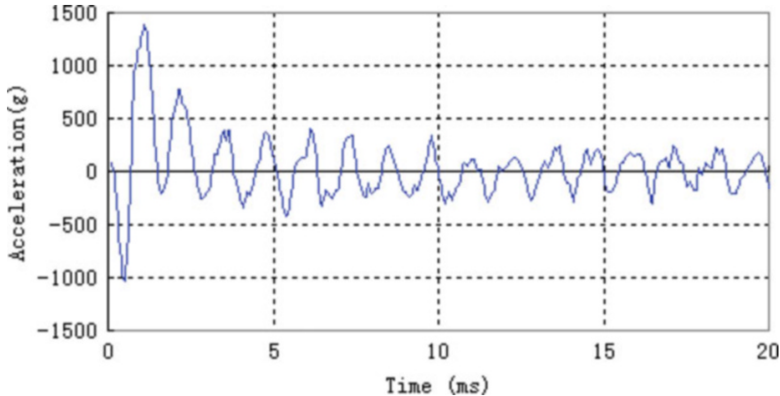

Fig. 7.28 Acceleration–time relationship of the center point on specimen

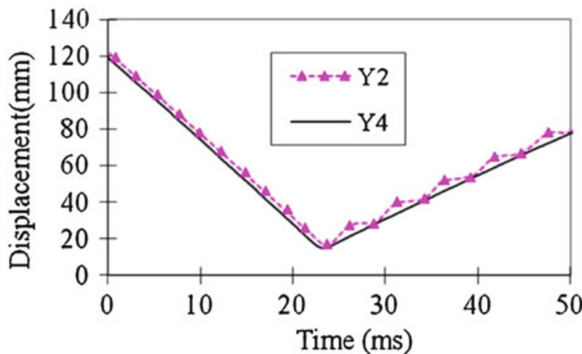

Fig. 7.29 Location of mark 2 and 4 measured by camera

The displacement period of the first transient cycle of the specimen agrees with first order vibration mode frequency for the clamped–clamped board. The vibration amplitude has good agreement with measured result, as the vibration amplitude is less sensitive to drop base impact condition compared to acceleration.

After drop impact, the transient vibration occurs. In order to find the stress strain behavior of solder joint, the component including solder joint must be modeled in FEA simulation. In this study, hybrid model was used to calculate the stress–strain behavior of FCOB solder joints subjected to impact loading. This method simulates the FCOB assembly without considering whole drop table, drop base, and fixture. The displacement of fixture measured by high-speed camera (see Fig. 7.29) was considered as the input boundary condition, applied along the fixed edges of specimen.

Explicit finite element analysis for FCOB assembly was conducted using LS-DYNA. In order to reduce the simulation time, only one large component near the board center numbered 4 was considered and mass scaling technique was used.

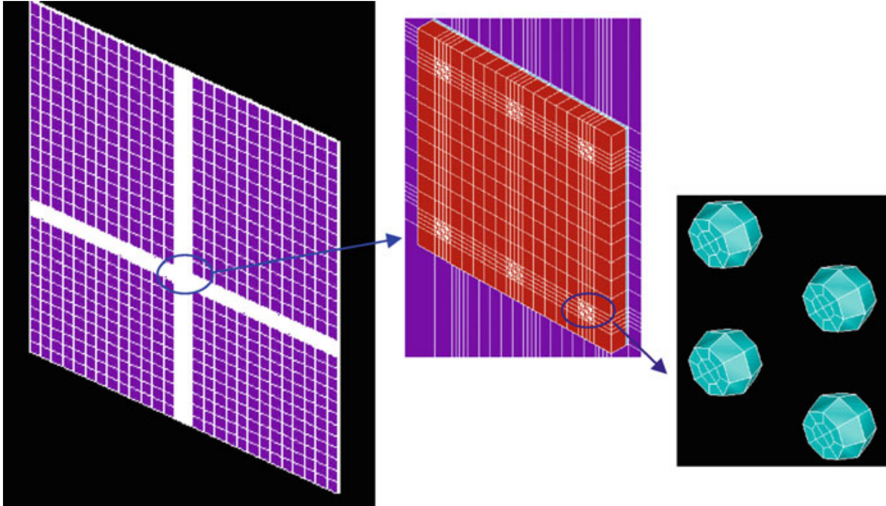

Fig. 7.30 FE model for FCOB assembly

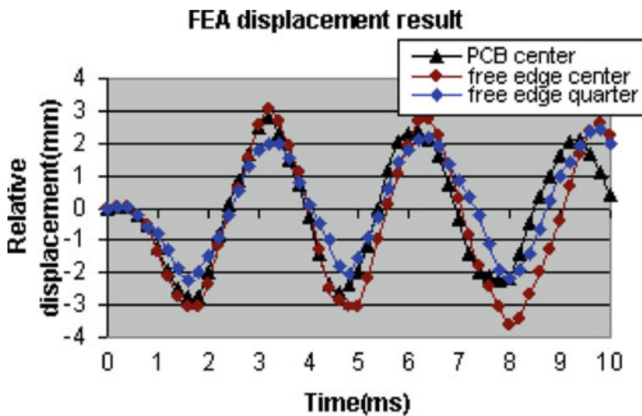

Fig. 7.31 FEA displacement result for drop test

Four different materials are considered in this simulation, including FR-4 PWB board, underfill, eutectic Sn/Pb solder, and silicon chip. Solder material was modeled as bilinear plastic behavior based on data derived from impact testing of solder. Figure 7.30 shows the FEA model for drop test simulation; corner solder balls are simulated in this model due to their critical location.

The displacement FEA result is shown in Fig. 7.31 for three points of PWB center, free edge center, and free edge quarter. Free edge center and free edge quarter in FEA result are corresponded to mark 2 and mark 3, as shown in Fig. 7.17, respectively. Comparing FEA result with testing result, it can be seen the relative displacement amplitude and vibration period has good agreement. Figure 7.32 shows the displacement and acceleration change with time on specimen center.

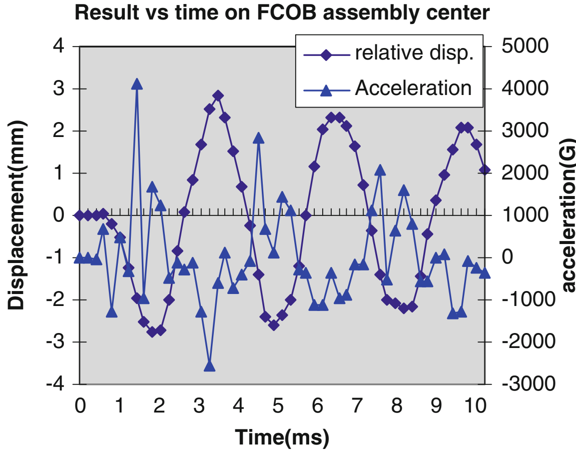

Fig. 7.32 Acceleration, displacement versus time

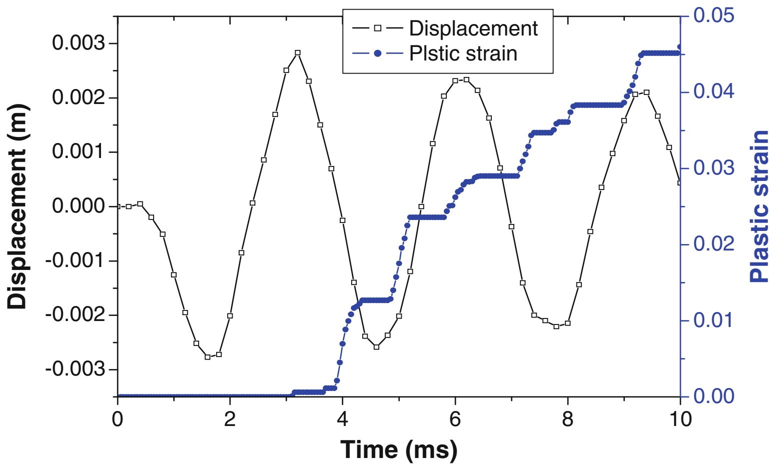

Fig. 7.33 Plastic strain, displacement versus time

It can be seen that the positive acceleration occurs when specimen bends down while the negative acceleration occurs when specimen bends up. The acceleration value calculated from FEA is slightly higher than that from the test result.

Figure 7.33 shows the plastic strain and displacement comparison with respect to time for one critical element of corner solder joint. It can be seen that when PWB first bent down no plastic deformation occurred. When PWB first got its peak bending-up point, plastic deformation occurred. Therefore, from this point, the cyclic plastic strain is calculated, and plastic strain of 0.02764 for first cycle and 0.01692 for second cycle are estimated. The cyclic plastic strain becomes lower with time due to damping.

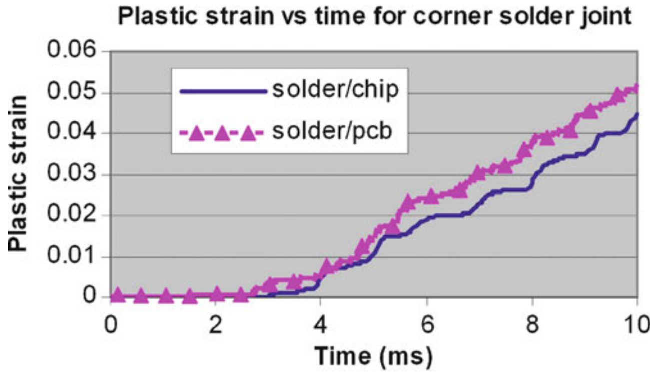

Fig. 7.34 Plastic strains of outmost corner solder joint

The volume-average method for plastic strain was used for the outermost corner elements of the corner solder joint because the plastic strain was very location-dependent. Figure 7.34 shows the volume-average plastic strain for outmost corner solder joint. It can be seen that the plastic strain on the solder/PWB side is more than that on the solder/chip side because PWB board flexure and inertial force have significant effect on solder material deformation near the PWB side while the board flexure effect is slighter for solder material deformation near the chip side than that near the PWB side.

When the plastic strain is obtained, the fatigue life of solder joint can be predicted based on the fatigue failure model such as Coffin–Manson model, which was used for lower cycle fatigue behavior of eutectic solder as shown below:

$$N_{\mathrm{f}}{}^{m}\Delta\varepsilon_{p} = C, \tag{7.11}$$

where C and m are material constants, which can be determined by polynomial expression fitting from temperature-dependent experimental data given by Shi et al. [24]. Using room temperature, $T = 25$, and frequency of 1 Hz obtain $m = 0.727$ and $C = 2.033$. There is a need for a suitable drop fatigue model. Tentatively, the Coffin–Manson model was used for drop fatigue life prediction. A time period of 10 ms was used for drop test analysis to calculate the solder joint drop plastic strain. The plastic strain equal to 0.0512 computed from solder/PWB side as shown in Fig. 7.34. The fatigue life, N_{f}, is equal to 158 drops. This means that after 158 drops from a drop height of 1 m, the solder joint on the FCOB assembly is subjected to plastic strain cycling due to the impact loading and is expected to fail by fatigue.

7.3.1 Drop Test for Pb-Free 95.5Sn–3.8Ag–0.7Cu Soldered Assembly

In this drop test, bare PCB and populated PCB were selected as drop specimens. For populated PCB specimen, one BGA, one QFP, and one TSSOP component are mounted on PCB board. For BGA component, three different surface finishes, such

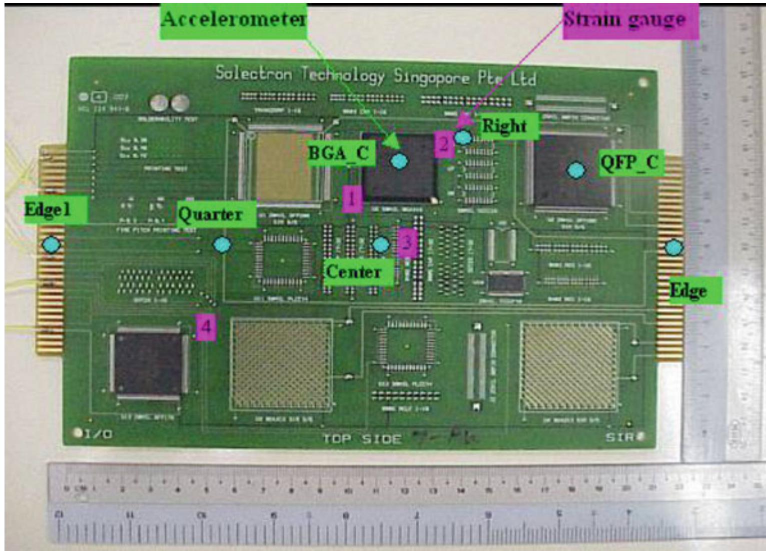

Fig. 7.35 Pb-free solder test board and measurement points

as Ag, Au, and OSP, are used. In the drop test, accelerometers and strain gauges were used to measure the dynamic response of the specimen subjected to drop loading. Figure 7.35 shows the locations of measurement. For bare PCB drop test, all four strain gauges were used, accelerations just on center and right location were measured, and four different drop heights were selected. For populated PCB specimen, all seven locations were selected for acceleration measurement and only strain gauge 1 and 2 near the BGA component were used. One-meter drop height for populated PCB specimen is fixed. For two different PCB specimens, the clamped–clamped boundary condition along the longer edge was used.

In populated PCB drop test, only 1 m-drop height was selected. Thirty drops were conducted for each surface-finishing component such as silver, gold, and OSP surface finishing. Figure 7.36 shows the acceleration comparison of PCB center for different surface finishing. Different surface finishing effect on acceleration can be ignored because it hardly affects the populated PCB structure, stiffness, and mass. Different surface finishing, however, can affect the fatigue failure of solder joint due to different interface material properties for different surface finishes. In this populated PCB drop test, seven different locations as shown in Fig. 7.36 were selected to measure the acceleration response. Figure 7.36 shows the acceleration of different locations for Ag surface finishing. Other surface finishes have almost same results. It can be seen from Fig. 7.37 that the largest acceleration will occur at PCB-free edge center. The acceleration on the QFP center is slightly more than that on BGA center because the location of the QFP center is closer to the free edge than location of BGA center. Thus can provide the guide to prevent the high acceleration of component mounted on PCB by arranging its location for clamped–clamped boundary condition.

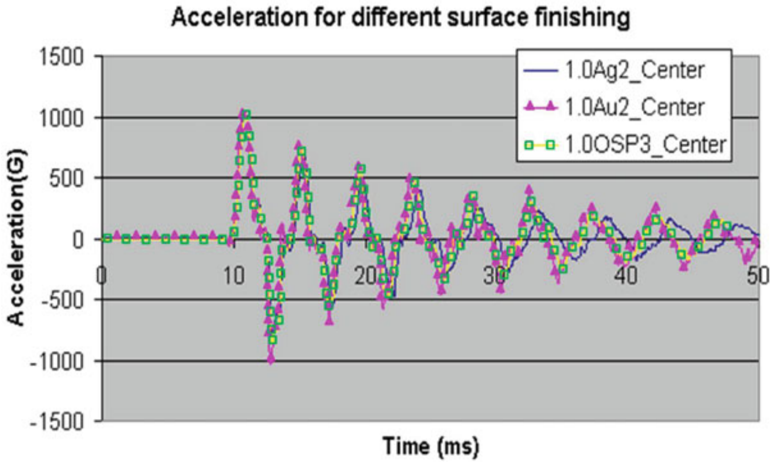

Fig. 7.36 Acceleration of PCB center for different surface finish

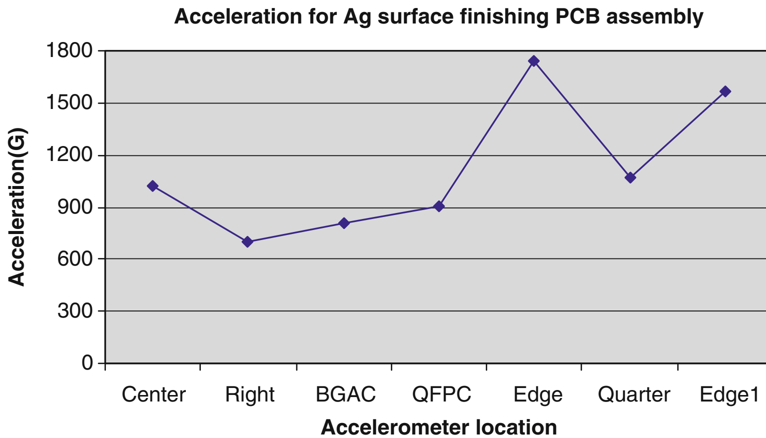

Fig. 7.37 Acceleration of different locations

In the populated PCB drop test, strain gauge 1 and 2 near the BGA corner as shown in Fig. 7.35 were used to measure the strain response of BGA component location. Figure 7.38 shows the strain result for three repeated measurements and the repeatability is consistent. In the drop test, the location of the accelerometer is changed after every five drops. The accelerometer has the mass of 2.4 g and this additional mass will affect the strain value when the accelerometer location varies. Figure 7.39 shows the effect of the accelerometer on the strain magnitude. It can be seen that the effect of accelerometer mass on strain of strain gauge1 is evident when accelerometer lay on the BGA center because of the added mass near the strain guage1 while the other locations effect is very slight.

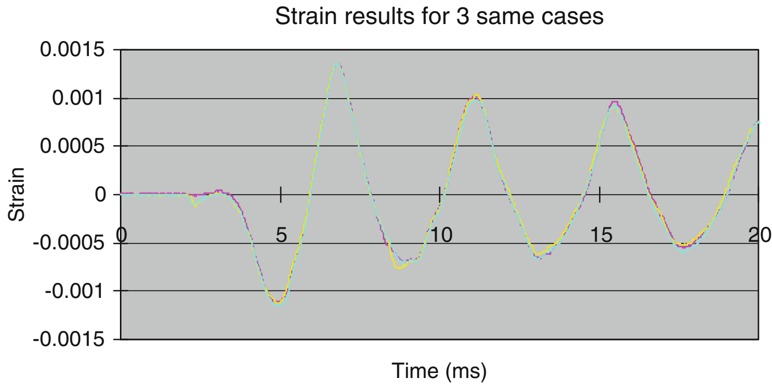

Fig. 7.38 Repeatability of strain measurement

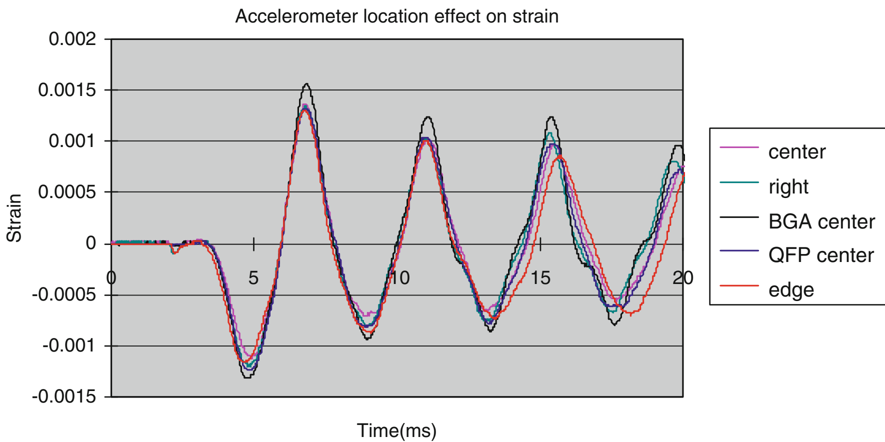

Fig. 7.39 Effect of accelerometer location on the strain

Figure 7.40 shows the strain comparison between strain gauge 1 and strain gauge 2 as shown in Fig. 7.35. It can be seen that the strain varies with position of PCB significantly and the strain magnitude becomes lower with time due to damping. Figure 7.41 shows the strain of strain gauge 1 for different surface finishing. It can be seen that the strain for the Au surface finishing is larger than that of others at the first PCB bending down while the strain will be almost same at subsequent PCB motion. Gold surface finishing PCB assembly indicates lower stiffness than other surface finishes when PCB is subjected to drop loading.

Reliability test for vibration fatigue was conducted for FCOB assembly with eutectic 63Sn–37Pb solder joints. Two methods of vibration fatigue analysis were developed using the G-level based *G*–*N* fatigue curve data for the FCOB assembly and the stress–life, *S*–*N* fatigue curve data for eutectic 63Sn–37Pb solder [25, 26].

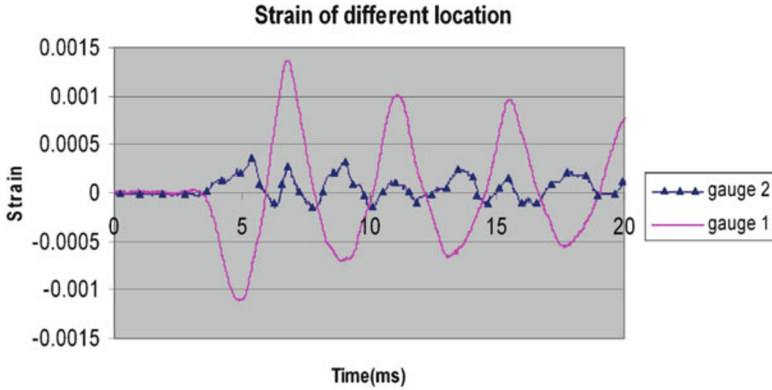

Fig. 7.40 Strain for different locations

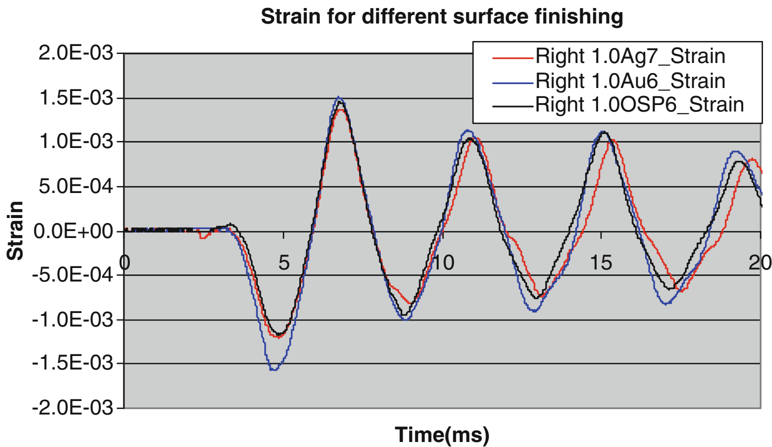

Fig. 7.41 Strain comparison for different boards

Drop impact test studies on the FCOB assembly with 63Sn–37Pb solder and Pb-free 95.5Sn–3.8Ag–0.7Cu soldered assemblies were conducted. Experimental measurements of the board-level displacement, acceleration, and strain responses were made. No failure was recorded after 30 drops from a 1-m height on the drop test machine [27].

Finite element analysis using the explicit dynamic analysis with LS-DYNA was able to model and simulate the board level deformation and acceleration characteristics. Stress and strain analysis of the solder joint was investigated for the FCOB assembly with 63Sn–37Pb solder and the predicted failure was estimated at 158 drops [26, 28].

References

1. Steinberg DS (1998) Vibration analysis for electronic equipment. Wiley, New York
2. Barker DB, Chen YS, Dasgupta A (1993) Estimating the vibration fatigue life of quad leaded surface mount components. J Electron Packaging 115:195–200
3. Pitarresi JM, Akanda A (1993) Random vibration response of a surface mount lead/solder joint. ASME international electronic conference, EEP, vol 4–1, Advances in electronic packaging, pp 207–215
4. Lee SB, Ham SJ (1999) Fatigue life assessment of bump type solder joint under vibration environment. ASME international electronic conference, EEP, vol 26–1, Advances in electronic packaging, pp 699–704
5. Yang QJ, Lim GH, Pang HLJ et al (1999) Vibration reliability analysis of a pbga assembly under foundation excitations. ASME international electronic conference, EEP, vol 26–1, Advances in electronic packaging, pp 705–711
6. Basaran C, Chandaroy R (1999) Nonlinear dynamic analysis of surface mount interconnects: Part I-theory. J Electron Packaging 121:8–11
7. Basaran C, Chandaroy R (1999) Nonlinear dynamic analysis of surface mount interconnects: Part II-application. J Electron Packaging 121:12–17
8. Chandaroy R, Basaran C (1999) Damage mechanics of surface mount technology solder joints under concurrent thermal and dynamic loading. J Electron Packaging 121:61–68
9. Zhao Y, Basaran C, Cartwright A, Dishongh T (2000) Thermomechanical behavior of micron scale solder joints under dynamic loads. Mech Mater 32:161–173
10. Meirovitch L (1986) Elements of vibration analysis. McGraw-Hill, New York
11. Yang QJ, Wang ZP, Lim GH et al (2002) Reliability of PBGA assemblies under out-of-plane vibration excitation. IEEE Trans Component Packaging Technol 25:293–300
12. Miner MA (1945) Cumulative fatigue damage. ASME J Appl Mech 12(3):A159–A164
13. Yao QZ, Qu JM, Wu SX (1999) Solder fatigue life in two chip scale packages. Proceedings of IEEE-IMAPS international symposium on microelectronics, Chicago, IL, October 1999, pp 563–570
14. Suhir E (2002) Could shock test adequately mimic drop test conditions? J Electron Packaging 24:170–177
15. Weaver W Jr, Timoshenko SP, Young DH (1990) Vibration problems in engineering. Wiley, New York
16. Sidharth V, Gannamani R, Zhang ML (2000) Characterization of a novel fine-pitch ball grid array package for flash memory application. Proceedings of 50th electronic components and technology conference, pp 353–357
17. Yu Q, Kikuchi H, Ikeda S, Shiratori M, Kakino M, Fujiwara N (2002) Dynamic behavior of electronics package and impact reliability of BGA solder joints. Proceedings of intersociety conference on thermal phenomena, pp 953–960
18. Xie DJ, Arra M, Yi S, Rooney D (2003) Solder joint behavior of area array packages in board level drop for handheld devices. Proceedings of 53rd of electronic component and technology conference, pp 130–135
19. Tee TY, Ng HS, Lim CT, Pek E, Zhong ZW (2003) Board level drop test and simulation of TFBGA packages for telecommunication applications. Proceedings of 53rd of electronic component and technology conference, pp 121–129
20. Masazumi M, Toyoda Y, Tajima T (2003) High solder joint reliability with lead free solders. Proceedings of 53rd of Electronic component and technology conference, pp 317–322
21. Zhu LP (2003) modeling technique for reliability assessment of portable electronic product subjected to drop impact loads. Proceedings of 53rd of electronic component and technology conference, pp 100–104
22. Lim CT, Ang CW, Tan LB, Seah SKW, Wong EH (2003) Drop impact survey of portable electronic products. Proceedings of 53rd of electronic component and technology conference, pp 113–120

23. Johnson W (1972) Impact strength of material. Edward Arnold, London
24. Shi XQ, Pang HLJ, Zhuo W, Wang ZP (2000) Low cycle fatigue analysis of temperature and frequency effects in eutectic solder alloy. Int J Fatigue 22:217–228
25. Che FX, Pang HLJ, Wong FL, Lim GH, Low TH (2003) Vibration fatigue test and analysis for flip chip solder joints. Proceedings of 5th EPTC conference, Singapore, 10–12 Dec 2003, pp 107–113
26. Pang JHL, Che FX, Low TH (2004) Vibration fatigue analysis for FCOB solder joints. Proceedings of 54th ECTC conference, Las Vegas, June 1–4 2004
27. Wang YQ, Low KH, Che FX, Pang HLJ, Yeo SP (2003) Modeling and simulation of printed circuit board drop test. Proceedings of 5th EPTC conference, Singapore, 10–12 Dec 2003, pp 263–268
28. Pang JHL, Low TH, Xiong BS, Che FX (2003) Design For reliability (DFR) methodology for electronic packaging assemblies. Proceedings of 5th EPTC conference, Singapore, 10–12 Dec 2003, pp 470–478